MicroRNA based feedforward control of intrinsic gene expression noise

Pavol Bokes, Michal Hojcka and Abhyudai Singh

Abstract—Intrinsic noise, which arises in gene expression at low copy numbers, can be controlled by diverse regulatory motifs, including feedforward loops. Here we study an example of a feedforward control system based on the interaction between an mRNA molecule and an antagonistic microRNA molecule encoded by the same gene, aiming to quantify the variability (or noise) in molecular copy numbers. Using linear noise approximation, we show that the mRNA noise is sub-Poissonian in case of non-bursty transcription, and exhibits a nonmonotonic response both to the species natural lifetime ratio and to the strength of the antagonistic interaction. Additionally, we use the Chemical Reaction Network Theory to prove that the mRNA copy number distribution is Poissonian in the absence of spontaneous mRNA decay channel. In case of transcriptional bursts, we show that feedforward control can attenuate the super-Poissonian gene-expression noise that is due to bursting, and that the effect is more considerable at the protein than at the mRNA level. Our results indicate that the strong coupling between mRNA and microRNA in the sense of burst stoichiometry and also of timing of production events renders the microRNA based feedforward motif an effective mechanism for the control of gene expression noise.

Index Terms—transcription bursts, mRNA noise, incoherent feedforward loop, noise reduction, linear noise approximation, Poisson distribution, chemical reaction network theory, product form distribution

1 Introduction

Gene expression requires the transcription of the information encoded on a gene into an mRNA molecule, followed by the translation of the mRNA molecule into a protein (Fig 1a). These processes can be a source of substantial variability if the constituent molecules are present at low copy numbers and/or they are produced in bursts [1]–[4]. Cells have evolved diverse mechanisms to counter stochasticity arising from gene expression. Negative feedback realized via gene autoregulation provides some of the most widely recognised examples [5]–[12]. A protein with negative feedback loop inhibits its own transcription or translation [13]–[16]. Surprisingly, negative autoregulation is relatively rare in eukaryotic transcription factors [17]. One plausible explanation is that the noise reduction capability of negative feedback deteriorates as a result of the delays incurred in transporting the protein from the eukaryotic cytoplasm.

The incoherent feedforward architecture provides an attractive alternative noise-supression mechanism (Fig 1b). Feedforward loops maintain desired expression level even if subjected to varying gene dosage [18] or upstream transcription factor concentrations [19]–[23]. Mounting biological evidence shows that, in many eukaryotic genes, the transcribed intronic regions that are removed during splicing are further processed to make a microRNA that targets the same gene's mRNA [24]. This mechanism constitutes a feedforward loop at the level of the gene, the mRNA transcript, and its microRNA antagonist (Fig 1c). The strong coupling between the mRNA and microRNA species both in the sense of stoichiometry and also of production timing suggests that the motif can be beneficial in reducing gene-expression noise.

Systems of chemical kinetics provide a suitable framework for the representation of genetic regulatory circuits. Exact probability mass functions of the reaction species copy numbers are however only rarely available [25]–[27]. The Chemical Reaction Network Theory specifies a class of systems operating at a complex-balanced equilibrium, which admit tractable product-form distributions [28]–[31]. Additionally, steady state copy number distributions in certain simple models that fall outside of the remit of the Chemical Reaction Network Theory can be characterised analytically in terms of the generating functions [32]–[34], [34]–[37]. If exact results are unavailable or intractable, asymptotic and approximation methods can provide useful insights into probabilistic behaviour of reactant copy numbers. The linear-noise approximation (LNA) and moment-closure methods can provide valuable approximations for the species means, variances and covariances, or even quantities based on higher-order moments [38]–[44].

The aim of this paper is to apply computational and mathematical methodologies to analyse a stochastic model of a feedforward loop with microRNA based control [45]–[48]. The model is represented by a reaction system, which is formally introduced in Section 2. Its essential features, both for the nonbursty and bursting cases, are identified in Section 3. The same Section contains a comparison of the model with three other circuits: the unregulated (or constitutive) gene expression model; and two alternative microRNA based regulation models with a relaxed coupling in mRNA–microRNA production. Section 4 provides details

- *P. Bokes is and M. Hojcka was with the Department of Applied Mathematics and Statistics, Comenius University, Bratislava 84248, Slovakia. E-mail: pavol.bokes@fmph.uniba.sk*
- *A. Singh is with Department of Electrical and Computer Engineering, University of Delaware, Newark, Delaware 19716, USA.*

Manuscript received . . .; revised August . . ..

This article has been accepted for publication in a future issue of this journal, but has not been fully edited. Content may change prior to final publication. Citation information: DOI 10.1109/TCBB.2019.2938502, IEEE/ACM Transactions on Computational Biology and Bioinformatics

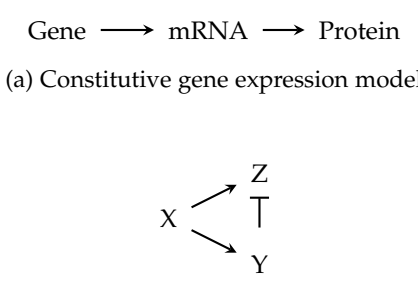

(a) Constitutive gene expression model

(b) Universal representation of an incoherent feedforward loop

(c) microRNA based regulation

Fig. 1: 1a. In the constitutive gene expression model, the gene information is transcribed onto an mRNA molecule which is then translated into a protein. 1b. In a general formulation of an incoherent feedforward loop, a species X activates species Y and Z, and the species Y represses species Z. 1c. In microRNA based regulation, a gene encodes mRNA and microRNA, and microRNA degrades mRNA. The gene, mRNA, and microRNA triangle form the basic feedforward structure in the microRNA regulatory motif.

for the LNA results and cross-validates them with large-scale kinetic Monte Carlo simulations. The paper concludes in Section 6 with a summary and discussion of the presented results.

2 THE STATEMENT OF THE MODEL

The feed-forward model that we consider here is a discrete stochastic chemical kinetics system composed of three species P (protein), X (mRNA) and Y (microRNA) which are subject to seven reaction channels

$$\begin{aligned} &R_1 : \emptyset \xrightarrow{k} B \times (\mathrm{X}+\mathrm{Y}), \quad R_2 : \mathrm{X}+\mathrm{Y} \xrightarrow{\frac{\delta(1-q)}{k}} \emptyset, \\ &R_3 : \mathrm{X}+\mathrm{Y} \xrightarrow{\frac{\delta q}{k}} \mathrm{Y}, \qquad R_4 : \mathrm{Y} \xrightarrow{1} \emptyset, \quad R_5 : \mathrm{X} \xrightarrow{\varepsilon} \emptyset, \\ &R_6 : \mathrm{X} \xrightarrow{\lambda} \mathrm{X}+\mathrm{P}, \qquad R_7 : \mathrm{P} \xrightarrow{\mu} \emptyset. \end{aligned} \tag{1}$$

The reaction R_1 represents the transcription of a burst of mRNA–microRNA pairs. Note that the timing and the stoichiometry of mRNA and microRNA production is strongly coupled in the reaction R_1. The transcriptional burst size B is drawn from a random distribution

$$P[B=i] = b_i, \quad i = 1, 2, \ldots, \tag{2}$$

where $b_1 + b_2 + \ldots = 1$. The geometric distribution

$$b_i = (1-p)^{i-1}p, \quad i = 1, 2, \ldots, \tag{3}$$

is commonly used, and can be justified by a random-trial model with failure probability p, in which molecular pairs are successively transcribed until the first failure event occurs.

Reaction	Reaction vector	Reaction rate
$R_1^{(1)} : \emptyset \xrightarrow{kb_1} X+Y$	$(0,1,1)$	kb_1
$R_1^{(2)} : \emptyset \xrightarrow{kb_2} 2\times(X+Y)$	$(0,1,1)$	kb_2
$\vdots$	$\vdots$	$\vdots$
$R_1^{(i)} : \emptyset \xrightarrow{kb_i} i\times(X+Y)$	$(0,i,i)$	kb_i
$\vdots$	$\vdots$	$\vdots$
$R_2 : \mathrm{X}+\mathrm{Y} \xrightarrow{\frac{\delta(1-q)}{k}} \emptyset$	$(0,-1,-1)$	$\frac{\delta(1-q)XY}{k}$
$R_3 : \mathrm{X}+\mathrm{Y} \xrightarrow{\frac{\delta q}{k}} \mathrm{Y}$	$(0,-1,0)$	$\frac{\delta qXY}{k}$
$R_4 : \mathrm{Y} \xrightarrow{1} \emptyset$	$(0,0,-1)$	Y
$R_5 : \mathrm{X} \xrightarrow{\varepsilon} \emptyset$	$(0,-1,0)$	εX
$R_6 : \mathrm{X} \xrightarrow{\lambda} \mathrm{X}+\mathrm{P}$	$(1,0,0)$	λX
$R_7 : \mathrm{P} \xrightarrow{\mu} \emptyset$	$(-1,0,0)$	μP

TABLE 1: Reaction vectors and rates for the reaction channels of the feedforward model (1). A reaction vector gives the changes in molecular copy numbers of P (protein), X (mRNA), and Y (microRNA), respectively, that are induced by the given reaction. The reaction rate gives the probabilistic intensity of reaction occurrence.

Given that the product stoichiometry is drawn from a random distribution (2), the bursty production reaction channel R_1 is not an elementary reaction. However, since theory has been developed especially for systems of elementary reactions, it is advantageous to rewrite the non-elementary reaction channel R_1 into an infinite series

$$R_1^{(i)} : \emptyset \xrightarrow{kb_i} i \times (X+Y), \quad i = 1, 2, \ldots, \tag{4}$$

of elementary reactions, each corresponding to one potential realisation of burst size.

The other reaction channels in (1) have the following interpretations. In the reaction channels R_2 and R_3, a pair of X and Y molecules interact, which leads to the elimination of X; the Y molecule survives its antagonistic action on X with probability q, where $0 \leq q \leq 1$ are allowed. For studies with a decoupled production of X and Y and $q = 0$ we refer the reader e.g. to [25]–[27]. Note that the reaction rates of the two second-order reaction channels R_2 and R_3 are divided by k in order to achieve a classical scaling [49] with respect to the parameter k. Doing so makes the ensuing analysis more transparent.

The reaction channels R_4 and R_5 describe the spontaneous degradation of Y and X. By measuring time in units of the expected lifetime of Y, we are able to fix the reaction constant of R_4 to one. The parameter ε gives the ratio of Y to X lifetimes. In particular, small values of ε pertain to the assumption that X be much more stable than Y. Finally, the reaction channel R_6 corresponds to the translation of protein from an mRNA transcript, and the reaction channel R_7 characterises the protein decay.

The basic characteristics of the reaction system (1) are succinctly summarised in Table 1. For each reaction, we report its reaction vector and reaction rate. The reaction vector gives the changes in molecular copy numbers that are triggered by the occurrence of the reaction. The reaction

This article has been accepted for publication in a future issue of this journal, but has not been fully edited. Content may change prior to final publication. Citation information: DOI 10.1109/TCBB.2019.2938502, IEEE/ACM Transactions on Computational Biology and Bioinformatics

rate, when multiplied by the length $\mathrm{d}t$ of a small time differential, gives the probability that the reaction occurs within the small time interval. The reaction rate is obtained by multiplying the number of possible reactant combinations with the appropriate reaction rate constant.

3 Main Results

In this section we explain how the choice of kinetic parameters in (1) affects the stochastic noise in the X and P copy numbers at steady state. We use the Fano factor, which is defined as the ratio of the variance to the mean, as our chosen noise metric of molecular copy number noise. It is well known that the Fano factor is equal to one for the Poisson distribution. We refer to a distribution with Fano factor lower than one (greater than one) as sub-Poissonian (super-Poissonian). The formulae provided in this section as well as numerical results presented in the accompanying figures are based on the linear noise approximation (LNA), the derivation of which follows in Section 4. For greater clarity, we separately treat the nonbursty case ($B = 1$ with probability one) and bursty case (with a general distribution of B).

3.1 Nonbursty case

In the nonbursty regime, we obtain for the mRNA Fano factor a tractable formula

$$F_{\mathrm{X}} = 1 - \frac{\varepsilon\delta}{(\varepsilon+\delta)^2(1+\varepsilon+\delta)} \quad \text{for } q = 1 \text{ and } B = 1. \quad (5)$$

Note that the LNA result (5) is independent of the system size parameter k. The function (5) is visualised as a heat map in the left panel of Fig 2a.

Elementary analysis of (5) reveals that

1) The steady-state distribution of X is sub-Poissonian if $\varepsilon > 0$ and $\delta > 0$.
2) If there is no interaction ($\delta = 0$) or if X is stable ($\varepsilon = 0$), the Fano factor is equal to one.
3) For a fixed positive value of ε, the Fano factor is a nonmonotonic function of δ, initially decreasing before reaching a minimum, and slowly increasing back to one as $\delta \to \infty$.
4) The analogous holds if the roles of ε and δ are reversed in Property 3.
5) The function $F_{\mathrm{X}}(\varepsilon, \delta)$ is discontinuous at $(\varepsilon, \delta) = (0, 0)$. A range of limiting values can be achieved depending on along which ray the origin is approached.
6) The function $F_{\mathrm{X}}(\varepsilon, \delta)$ does not have an unconstrained minimum. An infimum of 0.75 is approached if $\varepsilon = \delta \to 0$.

The function F_{X} can be efficiently evaluated also for $0 \leq q < 1$, but the algebra reveals little. Graphical examination of F_{X} indicates that all the above properties hold for $0 < q \leq 1$ (see the right panel of Fig 2a for $q = 0.5$). The infimum of the Fano factor in Property 6 is lower than 0.75 if $q < 1$ and is approached along a different ray emanating from the origin. In the exceptional case $q = 0$ the dependence of F_{X} on ε and δ is monotonous.

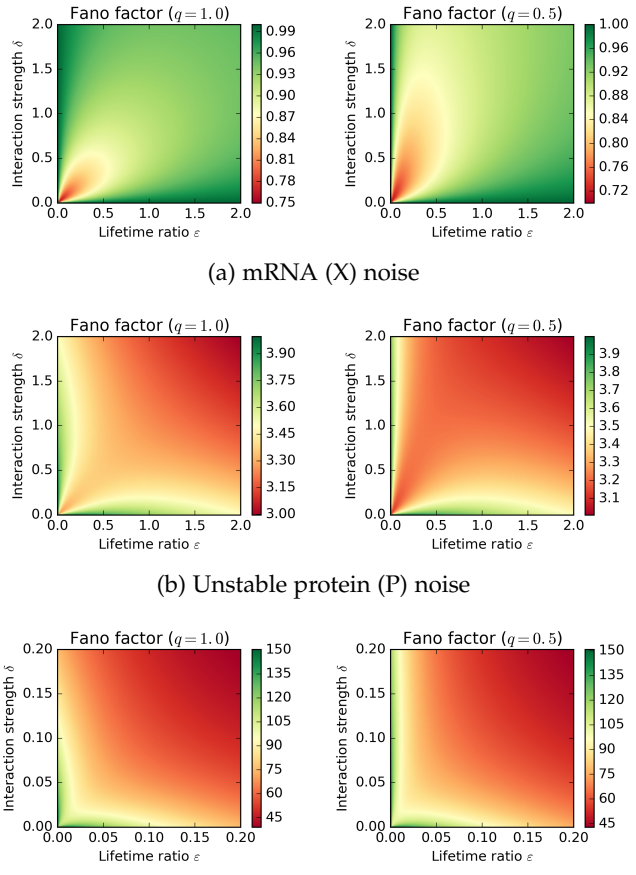

(a) mRNA (X) noise

(b) Unstable protein (P) noise

(c) Stable protein (P) noise

Fig. 2: Linear noise approximation based Fano factor of species X (mRNA; top panels) and P (protein; central and bottom panels) in the nonbursty case as functions of model parameters. In the left-hand side panels, $q = 1$ means that species Y (microRNA) survives its antagonistic action on species X (mRNA), whereas in the right-hand side panels, it survives with probability $q = 0.5$. The translation rate is set to $\lambda = 30$ and the protein decay rate constant is set to $\mu = 10$ (Fig 2b) or $\mu = 0.2$ (Fig 2c) (all rates are scaled by the decay rate constant of Y).

Property 2 suggests, but does not provide a definitive proof, that the distribution of X is Poissonian if $\varepsilon = 0$ or $\delta = 0$. In the non-interaction case ($\delta = 0$), the proof is straightforward: the dynamics of X is that of a simple immigration-and-death process, which is known to generate a Poisson distribution [50]–[52]. If X is stable ($\varepsilon = 0$), the distribution is again Poisson, but the proof requires a more subtle reasoning based on the Chemical Reaction Network Theory. We present the details in Section 5.

The protein Fano factor is given in the nonbursty case by

$$F_{\mathrm{P}} = 1 + \frac{\lambda}{\mu+\delta+\varepsilon}\left(1 - \left(\frac{1}{\varepsilon+\delta} + \frac{1}{1+\mu}\right) \times \frac{\varepsilon\delta}{(\delta+\varepsilon)(1+\varepsilon+\delta)}\right) \quad \text{for } q = 1 \text{ and } B = 1. \quad (6)$$

Despite simplifying assumptions, the formula for the pro-

This article has been accepted for publication in a future issue of this journal, but has not been fully edited. Content may change prior to final publication. Citation information: DOI 10.1109/TCBB.2019.2938502, IEEE/ACM Transactions on Computational Biology and Bioinformatics

tein noise is considerably more intricate than its mRNA counterpart (5). The following conclusions can nevertheless be drawn.

1) If μ is large, i.e. if protein is unstable, and ε and δ are small or moderate at most, the protein Fano factor is approximately proportional to the mRNA Fano factor (compare the near-origin behaviour of heatmaps in Fig 2a and Fig 2b).
2) If ε or δ are large, the Fano factor slowly decreases to the Poissonian value of one (cf. Figs 2b and 2c). This is because increasing δ or ε leads to greater mRNA turnover which brings about an effective attenuation of translational bursts.
3) If μ is moderate or small, i.e. if the protein is stable, then the role of translation burst attenuation becomes the dominant one (Fig 2c).

The results for $0 < q < 1$, which are presented in the right hand side panels of Figs 2b and 2c, are obtained numerically (see Section 4), and are found to be in broad qualitative agreement with the situation observed for $q = 1$.

3.2 Bursty case

Recall that in the nonbursty case, the natural stability of X ($\varepsilon = 0$) implies Poissonian mRNA and microRNA noise ($F_{\mathrm{X}} = F_{\mathrm{Y}} = 1$). Contrastingly, the bursty regime generates super-Poissonian distributions with LNA-based Fano factor of

$$F_{\mathrm{X}} = 1 + \frac{\gamma B_{\mathrm{eff}}}{1+\gamma}, \quad F_{\mathrm{Y}} = 1 + B_{\mathrm{eff}} \quad \text{for } q = 1 \text{ and } \varepsilon = 0, \tag{7}$$

where

$$\gamma = \delta \langle B \rangle \tag{8}$$

is the mRNA turnover rate and

$$B_{\mathrm{eff}} = \frac{\langle B^2 \rangle - \langle B \rangle}{2\langle B \rangle} \tag{9}$$

is the effective burst size [53]. Elementary analysis shows that for geometrical distribution (3) the effective burst size satisfies $B_{\mathrm{eff}} = \langle B \rangle - 1$ (see Appendix Afor derivation).

The formula (7) implies, perhaps somewhat counter-intuitively, that in the absence of spontaneous mRNA decay increasing interaction strength δ leads to an increase in mRNA noise. The apparent paradox is explained by noting that according to (8) large interaction strengths imply a fast turnover of mRNA, which can render the molecule uncontrollable by the relatively more stable microRNA. Note also that equation (7) cannot be used for $\delta = 0$ (and at the same time $\varepsilon = 0$), since in this case the model (1) fails to possess a steady-state distribution.

For $\varepsilon > 0$ or $q \neq 1$ the algebraic form of the mRNA Fano factor is a complicated expression that reveals little. However, the inspection of numerically calculated values in Fig 3a implies that, for a fixed positive lifetime $\varepsilon > 0$, the mRNA Fano factor is a non-monotonous function of the interaction strength δ. Indeed, at low levels of interaction ($\delta \to 0$), noise increases because the spontaneous mRNA decay channel R_5 dominates the microRNA-driven mRNA decay channels R_2 and/or R_3; for high levels of interaction ($\delta \to \infty$), the large mRNA turnover rate renders the species

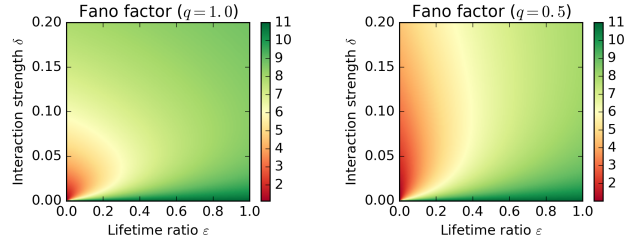

(a) mRNA noise

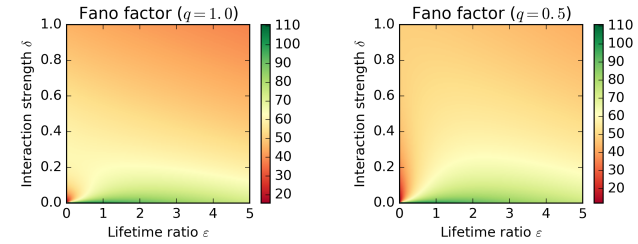

(b) Unstable protein noise

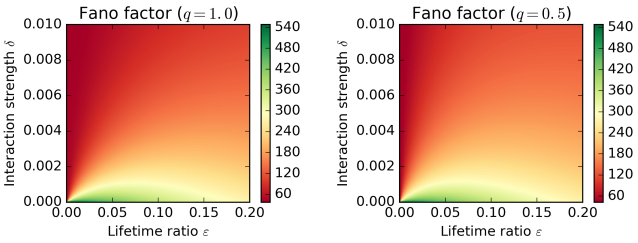

(c) Stable protein noise

Fig. 3: Linear noise approximation based Fano factor of species X (mRNA) and P (protein) in the bursty case as functions of model parameters. In the left-hand side panels, $q = 1$ means that species Y (microRNA) survives its antagonistic action on species X (mRNA), whereas in the right-hand side panels, it survives with probability $q = 0.5$. The burst size is geometrically distributed with $\langle B \rangle = 11$ so that $B_{\mathrm{eff}} = 10$ (see Appendix A). The protein production and decay rate constants are set to $\lambda = 100$, $\mu = 10$ (Fig 3b) and $\lambda = 10$, $\mu = 0.2$ (Fig 3c) (all rates are scaled by the decay rate constant of Y).

uncontrollable. Increasing the spontaneous mRNA decay rate ε leads to an increase in noise and a less effective performance of the feedforward circuit.

The LNA of the protein Fano factor is given for $q = 1$ and $\varepsilon = 0$ by the formula

$$F_{\mathrm{P}} = 1 + \frac{\lambda}{\gamma + \mu}\left(1 + \frac{\mu\gamma B_{\mathrm{eff}}}{(1+\mu)(1+\gamma)}\right). \tag{10}$$

Inspecting (10) and the numerically calculated values in Fig 3b–3c, we note that different qualitative results are obtained for unstable (Fig 3b) and stable (Fig 3c) proteins. For unstable protein (a large value of μ), the protein noise faithfully copies the mRNA noise for low to medium values of ε and δ, trailing off as δ or ε increase to infinity due to traslation burst attenuation (Fig 3b). For stable proteins, increasing the interaction strength reduces protein noise through the attenuation of translation bursts (Fig 3c).

This article has been accepted for publication in a future issue of this journal, but has not been fully edited. Content may change prior to final publication. Citation information: DOI 10.1109/TCBB.2019.2938502, IEEE/ACM Transactions on Computational Biology and Bioinformatics

3.3 Controlled comparison with a constitutive model

Here we consider a constitutive model for gene expression with transcriptional bursting to provide a benchmark for the evaluation of the performance of feedforward regulation introduced in the previous sections. The constitutive model is a reaction system with the protein (P) and mRNA (X) species being subject to reactions

$$\emptyset \xrightarrow{k} B \times X, \quad X \xrightarrow{\gamma} \emptyset, \quad X \xrightarrow{\lambda} X + P, \quad P \xrightarrow{\mu} \emptyset. \tag{11}$$

The reactions in (11) represent, in that order, bursting transcription of mRNA, decay of mRNA, translation of protein from an mRNA, and the decay of protein. The burst size B is drawn from a prescribed distribution (2) as in the feedforward loop model.

Aiming to provide a meaningful comparison between the feedforward (1) and constitutive (11) models, we make sure that both have the same rate of mRNA turnover. This can be achieved by equation (8) in the special tractable case of $q = 1$ and $\varepsilon = 0$; in the general case one uses $\gamma = \delta\tilde{y} + \varepsilon$, where δ is the interaction strength, ε is the spontaneous mRNA decay rate in the feedforward model, and $\tilde{y}$ gives the mean microRNA level (Section 4).

Usual techniques (see Appendix B) yield expressions for mRNA and protein Fano factors

$$F^0_{\mathrm{M}} = 1 + B_{\mathrm{eff}}, \quad F^0_{\mathrm{P}} = 1 + \frac{\lambda(1 + B_{\mathrm{eff}})}{\mu + \gamma}. \tag{12}$$

The zeros in the superscript of the Fano factors are meant to indicate the lack of regulation. Comparing (12) to its analogues (7) and (10) obtained for the feedforward model, we see that the microRNA-based regulation attenuates the effective burst size B_{eff} at the mRNA and protein stages. For the noise reduction to become important at the mRNA level, the turnover γ of the mRNA species must be sufficiently lower than the unit turnover of microRNA. At the protein level, a more substantial attenuation of noise can be achieved, as is manifested by the additional damping prefactor multiplying B_{eff} in (7). In particular, in a situation where mRNAs are less stable than microRNAs which are less stable than protein, a mediocre reduction of mRNA noise, accompanied however by a substantial reduction of protein noise, can follow.

Figure 4 reports the regulated-to-constitutive Fano factor ratios $F_{\mathrm{X}}/F^0_{\mathrm{X}}$ (left panel) and $F_{\mathrm{P}}/F^0_{\mathrm{P}}$ (right panel) as functions of the interaction strength δ. The feedforward model with strong coupling in mRNA and microRNA production 1 is thereby referred to as Model 1, and the other two models refer to certain modifications thereof, which are introduced in the following sections. Without spontaneous decay of mRNA ($\varepsilon = 0$), gene expression noise can be efficiently attenuated with feedforward control at sufficiently low interaction strengths (Figure 4, full blue line). If spontanoues decay of mRNA is enabled ($\varepsilon = 1$), the dependence of the relative noise on interaction strength becomes non-monotonous, with the baseline performance of one being obtained at low interaction strengths as well as high interaction strengths (Figure 4, dashed blue line). At the mRNA stage, this can severely limit the ability of feedforward circuit to reduce noise (Figure 4, left panel, blue line). At the protein stage, however, a substantial reduction

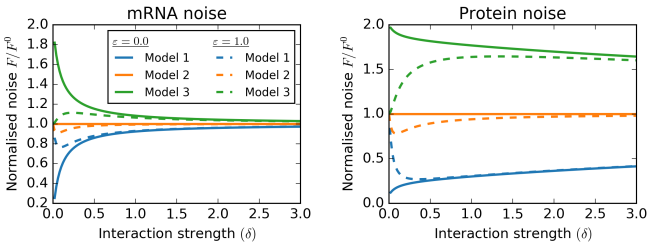

Fig. 4: Noise controlling performance of microRNA based regulation models. Three variants of regulation via microRNA are considered. Model 1 is the original formulation with strong coupling in burst timing and stoichiometry (cf. Equation 4). In Model 2 , the coupling in stoichiometry is removed (cf. Equation 14). In Model 3, mRNA and microRNA are independently produced (cf. Equation 18). The reported value of the normalised noise is defined as the ratio of the Fano factor F in a microRNA based regulation model to the referential Fano factor F^0 (12) based on a constitutive model of gene expression (11). The interaction strength δ is being varied and two choices of for the natural microRNA to mRNA lifetime ratio $\varepsilon \in \{0, 1\}$ are considered. The effective transcriptional burst size is set to $B_{\mathrm{eff}} = 10$ molecules. The probability of microRNA surviving its action on mRNA is set to $q = 1$. The translation rate is set to $\lambda = 10$ and protein decay rate constant is set to $\mu = 0.2$. All reaction constants are scaled with the microRNA decay rate constant.

can be obtained for a wide range of interaction strengths (Figure 4, right panel, blue line).

3.4 Decoupling burst stoichiometry

In the feedforward model (1), transcription bursts lead to the production of the same copy number of mRNA and microRNA. In order to quantify the importance of the coupling in stoichiometry, we modify the model (1) by replacing the first reaction with

$$R'_1 : \emptyset \xrightarrow{k} B \times R + \tilde{B} \times M, \tag{13}$$

where B and $\tilde{B}$ are two variates drawn from the burst size distribution (2) independently of each other. The bursting reaction (13) can equivalently be written as an infinite two-dimensional series

$$R'^{i,j}_1 : \emptyset \xrightarrow{kb_ib_j} i \times M + j \times B, \quad i = 1, 2, \ldots, \quad j = 1, 2, \ldots \tag{14}$$

of elementary chemical reactions. The mean behaviour of the feedforward model (see Section 4) is the same regardless whether the burst stoichiometries are coupled as in R_1 in (1) or independently chosen as in R'_1 in (13). The loss of coupling however affects the noise.

Calculations in Section 4 show that under the simplifying assumptions of $\varepsilon = 0$ and $q = 1$ the mRNA and microRNA Fano factors are given by

$$\begin{aligned} F_{\mathrm{X}} &= 1 + \frac{\gamma B_{\mathrm{eff}} + F_{\mathrm{b}}}{\gamma + 1}, \quad F_{\mathrm{Y}} = 1 + B_{\mathrm{eff}}, \\ F_{\mathrm{P}} &= 1 + \frac{\lambda}{\mu + \gamma}\left(1 + \frac{\gamma\mu B_{\mathrm{eff}} + (1 + \gamma + \mu)F_{\mathrm{b}}}{(1 + \gamma)(1 + \mu)}\right), \end{aligned} \tag{15}$$

Model type/Species	MicroRNA	mRNA	Protein
Strongly coupled mRNA–microRNA production (Sec. 3.2)	$1+B_{\rm eff}$	$1+\frac{\gamma B_{\rm eff}}{1+\gamma}$	$1+\frac{\lambda}{\mu+\gamma}\left(1+\frac{\mu\gamma B_{\rm eff}}{(1+\mu)(1+\gamma)}\right)$
Coupling in timing of production events (Section 3.4)	$1+B_{\rm eff}$	$1+\frac{\gamma B_{\rm eff}+F_{\rm b}}{1+\gamma}$	$1+\frac{\lambda}{\mu+\gamma}\left(1+\frac{\gamma\mu B_{\rm eff}+(1+\gamma+\mu)F_{\rm b}}{(1+\gamma)(1+\mu)}\right)$
Completely uncoupled mRNA/microRNA production (Section 3.5)	$1+B_{\rm eff}$	$\left(1+\frac{1}{1+\gamma}\right)(1+B_{\rm eff})$	$1+\frac{\lambda}{\mu+\gamma}\left(1+\frac{1+\mu+\gamma}{(1+\mu)(1+\gamma)}\right)(1+B_{\rm eff})$
Constitutive model (Section 3.3)	N/A	$1+B_{\rm eff}$	$1+\frac{\lambda(1+B_{\rm eff})}{\gamma+\mu}$

TABLE 2: Fano factors for the microRNA, mRNA, and protein species based on linear noise approximation. Results are provided for $\varepsilon=0$ (the spontaneous mRNA decay rate) and $q=1$ (the survival probability of microRNA after interacting with mRNA) in four separate models: the original feedforward model (first row) with coupling in both stoichiometry and timing; the two variants of the feedforward model (second and third rows) with coupling in timing only or no coupling at all; and the consitutive model (fourth row) without microRNA-based regulation. The parameters γ and μ give the rates of mRNA and protein turnover per molecule. All rates are scaled with microRNA decay rate constant. The parameter λ gives the translation rate. The parameter $B_{\rm eff}$ and $F_{\rm b}$ are the effective burst size and the burst size Fano factor.

where $B_{\rm eff}$ is defined by (9) and $F_{\rm b}$ is the burst size Fano factor, which is defined by

$$F_{\rm b}=\frac{\langle B^2\rangle-\langle B\rangle^2}{\langle B\rangle}. \tag{16}$$

Comparing (15) to (7) and(10), we note that removing the coupling between mRNA and microRNA burst stoichiometry leads to a deterioration in noise controlling capability of microRNA-based feedforward regulation (Fig. 4, orange lines). Specifically, if the burst size distribution is geometric (3), then $F_{\rm b}=B_{\rm eff}$ (see Appendix Afor details), and (15) reduces to the result (12) that is available in the absence of feedforward control.

3.5 Decoupling burst timing

Removing coupling in both stoichiometry and timing in the feed forward model, we replace the first reaction in (1) by two independent bursting productions

$$\emptyset\xrightarrow{k} B\times R,\quad \emptyset\xrightarrow{k}\tilde{B}\times M. \tag{17}$$

This can be rewritten in terms of two series

$$\emptyset\xrightarrow{kb_i} i\times M,\quad i=1,2,\ldots,\quad \emptyset\xrightarrow{kb_j} j\times M,\quad j=1,2,\ldots \tag{18}$$

of elementary reactions. Again, replacing synchronised bursting with independent, asynchronous bursting does not impact on the resulting mean dynamics (Section 4), but affects the noise behaviour.

The results for mRNA and protein Fano factors for $\varepsilon=0$ and $q=1$ are in this case summarised by equations

$$\begin{aligned}F_{\rm X}&=\left(1+\frac{1}{1+\gamma}\right)(1+B_{\rm eff}),\quad F_{\rm Y}=1+B_{\rm eff},\\ F_{\rm P}&=1+\frac{\lambda}{\mu+\gamma}\left(1+\frac{1+\mu+\gamma}{(1+\mu)(1+\gamma)}\right)(1+B_{\rm eff}).\end{aligned} \tag{19}$$

Thus, if coupling is removed both in burst stoichiometry and burst timing, the resulting motif leads to greater values of gene-expression noise than those in (12) which are obtained in the absence of microRNA based control (Fig. 4, green lines).

The microRNA, mRNA and protein variabilities in the strongly coupled, weakly coupled, and uncoupled models, as well as in the referential constitutive model, are summarised in Table 2.

4 Linear-noise approximation

The linear noise approximation (LNA) provides a method for an efficient evaluation of molecular copy number noise across the parameter space of the model. Here we provide details on the derivation of the approximation. The LNA of the mean behaviour is given by the law-of-mass-action formulation of the reaction system (1), which is

$$\begin{aligned}\dot{p}&=\lambda x-\mu p,\\ \dot{x}&=k\langle B\rangle-\frac{\delta xy}{k}-\varepsilon x,\\ \dot{y}&=k\langle B\rangle-\frac{\delta(1-q)xy}{k}-y,\end{aligned} \tag{20}$$

where

$$\langle B\rangle=\sum_{i=1}^{\infty} ib_i$$

is the mean transcription burst size. Setting the derivatives in (20) to zero and solving the resulting algebraic system in p, x, and y yield the stationary mean values

$$p=k\tilde{p},\quad x=k\tilde{x},\quad y=k\tilde{y}, \tag{21}$$

where

$$\begin{aligned}\tilde{p}&=\frac{\lambda\tilde{x}}{\mu},\\ \tilde{x}&=\frac{2\langle B\rangle}{\delta q\langle B\rangle+\varepsilon+\sqrt{(\delta q\langle B\rangle+\varepsilon)^2+4\delta\varepsilon(1-q)\langle B\rangle}},\\ \tilde{y}&=q\langle B\rangle+\varepsilon(1-q)\tilde{x}.\end{aligned} \tag{22}$$

Note that the means (21) scale with the production rate constant k.

In order to obtain the LNA of the variance, we need to determine the steady-state fluctuation and dissipation

This article has been accepted for publication in a future issue of this journal, but has not been fully edited. Content may change prior to final publication. Citation information: DOI 10.1109/TCBB.2019.2938502, IEEE/ACM Transactions on Computational Biology and Bioinformatics

matrices of the reaction system (1). The dissipation matrix $\boldsymbol{A}$ is equal to the linearisation matrix of the system (20), i.e.

$$\boldsymbol{A} = -\begin{pmatrix} \mu & -\lambda & 0 \\ 0 & \delta\tilde{y}+\varepsilon & \delta\tilde{x} \\ 0 & \delta(1-q)\tilde{y} & 1+\delta(1-q)\tilde{x} \end{pmatrix}. \quad (23)$$

The fluctuation matrix $\boldsymbol{B}$ is obtained in the following manner [54]: for each reaction channel in the reaction system (Table 1), we calculate the outer product of the reaction vector [55], [56] with itself, and multiply it by the (steady-state) reaction rate; then we sum the results over all reaction channels. In our particular example this leads to

$$\boldsymbol{B} = k\tilde{\boldsymbol{B}}, \quad \text{where}$$
$$\tilde{\boldsymbol{B}} = \begin{pmatrix} 2\mu\tilde{p} & 0 & 0 \\ 0 & \langle B^2\rangle + \langle B\rangle & \langle B^2\rangle + \langle B\rangle - \tilde{y} \\ 0 & \langle B^2\rangle + \langle B\rangle - \tilde{y} & \langle B^2\rangle + \langle B\rangle \end{pmatrix}, \quad (24)$$

where

$$\langle B^2\rangle = \sum_{i=1}^{\infty} i^2 b_i$$

is the second moment of the burst distribution (2). The fluctuation–dissipation theorem [57] states that the covariance matrix $\boldsymbol{\Sigma}$ of the random vector of steady-state X and Y copy numbers satisfies

$$\boldsymbol{A}\boldsymbol{\Sigma} + \boldsymbol{\Sigma}\boldsymbol{A}^{\intercal} + \boldsymbol{B} = 0, \quad (25)$$

i.e.

$$\boldsymbol{\Sigma} = k\tilde{\boldsymbol{\Sigma}}, \quad \text{where} \quad \boldsymbol{A}\tilde{\boldsymbol{\Sigma}} + \tilde{\boldsymbol{\Sigma}}\boldsymbol{A}^{\intercal} + \tilde{\boldsymbol{B}} = 0. \quad (26)$$

Equation (26) is also referred to as Lyapunov equation. We solved the Lyapunov system numerically using the `solve_lyapunov` routine from Python's scientific package `scipy.linalg`.

Our chosen metric of the noise, the Fano factor, is given by

$$F_{\mathrm{P}} = \frac{\Sigma_{11}}{p} = \frac{\tilde{\Sigma}_{11}}{\tilde{p}}, \quad F_{\mathrm{X}} = \frac{\Sigma_{22}}{x} = \frac{\tilde{\Sigma}_{22}}{\tilde{x}}, \quad F_{\mathrm{Y}} = \frac{\Sigma_{33}}{y} = \frac{\tilde{\Sigma}_{33}}{\tilde{y}}$$

for the protein, mRNA, and microRNA, respectively. Since both the mean and the variance of each species scale linearly with k, the Fano factors are independent of the parameter.

For $q = 1$, the steady state levels (22) simplify to

$$\tilde{p} = \frac{\lambda\tilde{x}}{\mu}, \quad \tilde{x} = \frac{\langle B\rangle}{\delta\langle B\rangle + \varepsilon}, \quad \tilde{y} = \langle B\rangle,$$

and the linearisation matrix (23) reduces to

$$\boldsymbol{A} = -\begin{pmatrix} \mu & -\lambda & 0 \\ 0 & \delta+\varepsilon & \frac{\delta}{\delta+\varepsilon} \\ 0 & 0 & 1 \end{pmatrix}.$$

The triangular structure of the linearisation matrix A makes explicit calculations feasible. A series of elementary but lengthy calculations lead to formulae (5), (6), (7), and (10) reported above in Section 3.

Two other variants of bursty production of mRNA and microRNA were introduced in Sections 3.4–3.5. Recall that in the variant in Section 3.4 the coupling between mRNA and microRNA burst stoichiometry is removed (cf. Equation (13)), and in Section 3.5 in addition to removing coupling in burst stoichiometry, the timing of mRNA and microRNA bursts is desynchronised (cf. Equation (17)). In the modified models, the mean dynamics continues to satisfy the rate equations 20. The dissipation matrix, which is obtained by linearising the rate equations 20, remains therefore also the same 23. The fluctuation matrix however changes and instead of 24 we find

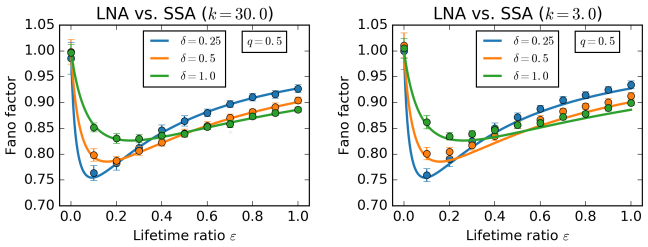

Fig. 5: The Fano factor of species X (mRNA) as function of model parameters as given by the linear-noise approximation (LNA, solid lines) and stochastic simulation algorithm (SSA, discrete markers). Two values of k are used, one large ($k = 30$, left panel) and one moderate ($k = 3$, right panel). The LNA is independent of k. Error bars indicate 99.9% confidence intervals for the simulation-based Fano factors.

$$\tilde{\boldsymbol{B}} = \begin{pmatrix} 2\mu\tilde{p} & 0 & 0 \\ 0 & \langle B^2\rangle + \langle B\rangle & \langle B\rangle^2 + \langle B\rangle - \tilde{y} \\ 0 & \langle B\rangle^2 + \langle B\rangle - \tilde{y} & \langle B^2\rangle + \langle B\rangle \end{pmatrix} \quad (27)$$

for the model with uncoupled burst stoichiometry (13) and

$$\tilde{\boldsymbol{B}} = \begin{pmatrix} 2\mu\tilde{p} & 0 & 0 \\ 0 & \langle B^2\rangle + \langle B\rangle & \langle B\rangle - \tilde{y} \\ 0 & \langle B\rangle - \tilde{y} & \langle B\rangle^2 + \langle B\rangle \end{pmatrix} \quad (28)$$

for the completely uncoupled production model (17). Comparing (24), (27), and (28) while noting that $0 \leq \langle B\rangle^2 \leq \langle B^2\rangle$ holds for burst size distributions, we gather that decoupling burst stoichiometry and/or timing leads to a decrease in the off-diagonal element in the fluctuation matrix. Such a decrease corresponds to an effective decrease of correlation between microRNA and mRNA production. The copy number covariance matrix $\boldsymbol{\Sigma}$ is calculated from the fluctuation dissipation theorem (26), where the dissipation matrix $\boldsymbol{A}$ is given by (23) and the fluctuation matrix $\tilde{\boldsymbol{B}}$ is given by (27) or (28) depending on which model version is being evaluated. The calculations lead to tractable results for $q = 1$ and $\varepsilon = 0$; for the remaining combinations of parameter values we prefer to use numerical evaluation of the Lyapunov equation (26).

A classical system-size-expansion argument [58] guarantees that the LNA accurately describes the reaction system (1) as k tends to infinity. We demonstrate the asymptotics in Fig 5, in which we compare the LNA of the mRNA Fano factor to the value obtained by the application of Gillespie's stochastic simulation algorithm (SSA) [59]. We observe a perfect agreement between the two if $k = 30$ (Fig 5, left panel). Although the agreement remains satisfactory for $k = 3$, the SSA results are now seen to deviate systematically from the LNA prediction for moderate values of ε and δ (Fig 5, right panel).

The reaction species mean values and standard deviations were calculated using Stochpy's [60] implementation

This article has been accepted for publication in a future issue of this journal, but has not been fully edited. Content may change prior to final publication. Citation information: DOI 10.1109/TCBB.2019.2938502, IEEE/ACM Transactions on Computational Biology and Bioinformatics

of Gillespie's direct method [59]. We skipped over the first 30 units of time to avoid the influence of an initial transient; we estimated the moments from the next 10^5 iterations (for $k = 3$) or 10^6 iterations (for $k = 30$) of the algorithm. The Fano factor was calculated as the ratio of the squared standard deviation to the mean value. The procedure was repeated to obtain 25 independent Fano factor estimates. The repetition increased accuracy and facilitated the construction of confidence intervals.

5 Stability of X implies Poisson distribution in the nonbursty case

In Section 4, we reported that provided that

1) production is nonbursty ($B = 1$),
2) X is stable ($\varepsilon = 0$),
3) Y has a chance of surviving the antagonism with X ($q > 0$),

then the linear noise approximation of the mRNA Fano factor is equal to one. Here we expand on this observation by providing an actual proof that the steady-state copy number of X (and also that of Y) follows the Poisson distribution. The argument is based on the application of the Chemical Reaction Network Theory (CRNT) [30].

Using the simplifying assumptions 1–3 in the chemical reaction system (1) and truncating to the mRNA (X) and microRNA species (Y) yields

$$\begin{aligned} &R_1 : \emptyset \xrightarrow{k} \mathrm{X} + \mathrm{Y}, \qquad R_2 : \mathrm{X} + \mathrm{Y} \xrightarrow{\frac{\delta(1-q)}{k}} \emptyset, \\ &R_3 : \mathrm{X} + \mathrm{Y} \xrightarrow{\frac{\delta q}{k}} \mathrm{Y}, \quad R_4 : \mathrm{Y} \xrightarrow{1} \emptyset, \end{aligned} \tag{29}$$

The combinations of reaction species appearing on the sides of reaction channels are referred as "complexes" in the CRNT framework [55]. The four reaction channels in (29) involve $N = 3$ complexes, namely the empty set $\emptyset$, the pair $\mathrm{X} + \mathrm{Y}$, and the singleton Y. The reaction system can be visualised as a graph whose vertices are the complexes of the reaction network and oriented edges represent reactions transforming one complex into another (Fig 6). In our current reaction graph, any two vertices can be connected by paths (a succession of oriented edges) in each direction. It follows that our reaction network is weakly reversible and covered by a single ($l = 1$) linkage class.

The reaction vectors span the entire two-dimensional ($s = 2$) space of X and Y copy number pairs. The deficiency of the reaction network is obtained by the well-known formula $\delta = N - l - s = 0$. According to CRNT [30], weakly reversible networks of zero deficiency admit a product-form steady-state distribution

$$P[X = m, Y = n] = C\frac{x^m y^n}{m!n!}, \tag{30}$$

where $x = k/\delta q$ and $y = kq$ are obtained by solving the law-of-mass action kinetics (20) at steady state, i.e. by setting $\varepsilon = 0$ and $\langle B \rangle = 1$ in (21)–(22).

Since the reaction system does not admit any conservation laws, the support of the distribution (30) includes all pairs of nonnegative integers $m, n \geq 0$. The normalisation constant C is then readily determined as $C = \mathrm{e}^{-x-y}$. In other words, the joint distribution of X and Y is the product of the marginal distributions, either of which is Poissonian with mean x and y, respectively.

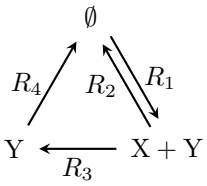

Fig. 6: Graphical representation of a reduced reaction system (29) obtained from (1) by disabling bursting and the spontaneous degradation of X (reaction channel R_5). The reduced reaction system is seen to be weakly reversible (unless $q = 0$). Additionally, it has zero deficiency and admits no conservation laws. Therefore, the copy numbers of X and Y are independent and Poissonian.

One of the powerful aspects of the Chemical Reaction Network Theory is that it generalises to complex extensions of Fig 6 as long as they do not violate its fundamental structural properties. Biologically, microRNAs tend to be promiscuous binders [61]. Below we extend the reaction network (29) (Fig 6) by an interaction between Y (the microRNA) and decoy binding sites. We show that the copy-number distributions remain Poissonian.

5.1 Extension of CRNT results to a system with decoy binding sites

The Chemical Reaction Network Theory (CRNT) can be applied to reaction networks that extend Fig 6 with additional reaction channels as long as they do not violate its fundamental structural properties. Assume, for example, that, in addition to reaction channels in (29), a molecule Y can bind to a free binding site B to form a heterodimer C, and that the heterodimer can dissociate into its constituents Y and B. Consider a reaction network obtained by extending that of Fig 6 by the reversible pair of reactions $\mathrm{Y} + \mathrm{B} \rightleftharpoons \mathrm{C}$. It is clear that the extended network remains weakly reversible, and that it involves $N = 5$ different complexes ($\emptyset$, $\mathrm{X} + \mathrm{Y}$, Y, $\mathrm{Y} + \mathrm{B}$, and C), which are interconnected within $l = 2$ linkage classes. The copy numbers (m, n, i, j) of the four reaction species (X, Y, C, and B) are constrained by the conservation law $i + j = \nu$, where ν gives the total number of binding sites. Consequently, the stoichiometric subspace has dimension $s = 4 - 1 = 3$, and the deficiency of the extended network is equal to $\delta = N - l - s = 5 - 3 - 2 = 0$. It follows that the steady-state distribution has the product form [30]

$$p_{m,n,i,j} = M\frac{x^m y^n c^i b^j}{m!n!i!j!}, \quad \text{for } i + j = \nu, \tag{31}$$

where

$$M = \left(\sum_{m\geq 0}\sum_{n\geq 0}\sum_{\substack{i,j\geq 0 \\ i+j=\nu}} \frac{x^m y^n c^i b^j}{m!n!i!j!} \right)^{-1} = \mathrm{e}^{-x-y}\frac{\nu!}{(c+b)^\nu} \tag{32}$$

is the normalisation constant. The first two components of the complex-balanced equilibrium (x, y, c, b) are still given

by the values $x = k/\delta q$ and $y = kq$ obtained in Section 5 in the absence of decoys. For the other two components of the complex-balanced equilibrium we have the balance condition $yb = Lc$, where L is the dissociation constant, and the conservation law $b + c = \nu$; solving in c and b yields

$$c = \frac{\nu y}{y + L}, \quad b = \frac{\nu L}{y + L}. \tag{33}$$

Inserting (33) into (31)–(32) and simplifying yields

$$p_{m,n,i,j} = \mathrm{e}^{-x-y} \frac{x^m y^n}{m!n!} \binom{\nu}{i} \frac{y^i L^{\nu-i}}{(y+L)^\nu}, \quad \text{for } i + j = \nu. \tag{34}$$

The distribution in (34) is a product of two Poissons for X and Y copy numbers and of a binomial for the number of heterodimers C. In particular, the distribution of X (mRNA) remains Poissonian despite the addition of an unspecific interaction with decoy binding sites.

6 Discussion

In this paper we considered a stochastic model for a feedforward loop driven by the interaction between mRNA and microRNA species. The model includes coupled production of mRNA and microRNA, their interaction, protein translation, and spontaneous decay of all molecular species. A distinction was made between non-bursty transcription, with a single microRNA–mRNA pair being transcribed at a time, and bursty transcription, in which two or more microRNA–mRNA pairs can be synthesised as a result of a single production event. The aim of the paper was to examine how the microRNA driven regulation impacts the mRNA and protein variability (noise) throughout the parameter space of the underlying computational model. Molecular noise was quantified using the Fano factor — the ratio of the variance (of a molecular species copy number) to its mean.

In the nonbursty case, our results reinforce the observation that feedforward regulation can buffer mRNA noise to sub-Poissonian levels [48]. The Fano factor exhibits a nonmonotonic behaviour: for a fixed microRNA to mRNA lifetime ratio, there is an optimal value of the interaction strength that minimises the Fano factor; conversely, for a fixed interaction strength, there exists an optimal lifetime ratio. Intriguingly, in the absence of spontaneous mRNA decay, the linear noise approximation based Fano factor is equal to the Poissonian value of one. We supported this observation with a conclusive proof, based on the Chemical Reaction Network Theory framework, that the mRNA copy-number distribution is Poissonian in the specific regime of nonbursty production and no spontaneous decay. The protein Fano factor exhibits qualitatively different behaviour depending on the stability of the protein. The noise in an unstable protein faithfully copies that of the upstream mRNA species, whereas for a stable protein the single most important effect is the control of translation burst size (number of protein molecules produced per mRNA molecule) through mRNA stability.

In the case of bursty transcription, mRNA distributions can be super-Poissonian, with large Fano factors being available in case of bursts of many molecular copies. Explicit calculations indicate that the bursting noise can be attenuated through feedforward control. In the absence of spontaneous mRNA decay, low interaction strengths lead to the Poissonian Fano factor value of one, whereas strong interactions imply an unregulated (large) value of Fano factor. Conceptually, the disadvantage of a large value of the interaction strength is that it leads to fast mRNA turnover which can interfere with feedforward control. If spontaneous mRNA decay is included, loss of noise control occurs both for low interaction strengths and large interaction strengths, and an optimal value of interaction strength can be found that minimises the mRNA Fano factor.

Our investigation indicates that the mRNA turnover rate (both spontaneous and driven by the interaction with microRNA) plays a crucial role in determining how much of the bursting noise is transmitted downstream to mRNA and protein levels. For this reason, we chose to compare the performance of the microRNA based feedforward model to a unregulated (or constitutive) model of bursty gene expression with the same mRNA turnover rate. The result is that the feedforward model leads to a lower value in both mRNA and protein noise, but that the reduction in protein noise can be much more substantial.

We argue that the strong coupling in burst stoichiometry and in the timing of production events is crucial for the noise reduction capability of the microRNA based feedforward circuit. Aiming to quantify the effect, we considered additional two microRNA based models, one in which timing of mRNA–microRNA bursts remains coupled but the burst stoichiometries are decoupled, and one in which the mRNA and microRNA production is entirely independent. Our results imply that removing the coupling in production worsens noise controlling capability of the system. In particular, removing the coupling in burst stoichiometry leads to the same noise as observed in the constitutive model, whereas the completely uncoupled case even leads to noise levels that exceed those observed in the absence of regulation.

In summary, we studied a stochastic feedforward loop motif featuring a coupled mRNA and microRNA production and an antagonistic interaction. We examined the consequences of the interaction on gene-expression noise in nonbursty as well as bursty transcription regimes. Using a combination of computational methodologies we characterised the model behaviour in several parameter regions of interest. We expect that analogous approaches will be helpful to understand other examples of intrinsically noisy gene-regulatory motifs operating at low copy numbers.

Acknowledgments

PB is supported by the Slovak Research and Development Agency under the contract No. APVV-18-0308 and by the VEGA grant 1/0347/18. AS is supported by the National Science Foundation grant ECCS-1711548.

References

[1] P. Swain, M. Elowitz, and E. Siggia, "Intrinsic and extrinsic contributions to stochasticity in gene expression," *P. Natl. Acad. Sci. USA*, vol. 99, no. 20, p. 12795, 2002.

[2] M. Elowitz, A. Levine, E. Siggia, and P. Swain, "Stochastic gene expression in a single cell," *Science*, vol. 297, pp. 1183–1186, 2002.

[3] A. Raj, C. Peskin, D. Tranchina, D. Vargas, and S. Tyagi, "Stochastic mRNA synthesis in mammalian cells," *PLoS Biol.*, vol. 4, p. e309, 2006.

[4] R. D. Dar, B. S. Razooky, A. Singh, T. V. Trimeloni, J. M. McCollum, C. D. Cox, M. L. Simpson, and L. S. Weinberger, "Transcriptional burst frequency and burst size are equally modulated across the human genome," *P. Natl. Acad. Sci. USA*, vol. 109, pp. 17454–17459, 2012.

[5] M. Voliotis and C. G. Bowsher, "The magnitude and colour of noise in genetic negative feedback systems," *Nucleic Acids Res.*, vol. 40, pp. 7084–7095, 2012.

[6] A. Singh and J. P. Hespanha, "Optimal feedback strength for noise suppression in autoregulatory gene networks," *Biophys. J.*, vol. 96, pp. 4013–4023, 2009.

[7] Y. Dublanche, K. Michalodimitrakis, N. Kummerer, M. Foglierini, and L. Serrano, "Noise in transcription negative feedback loops: simulation and experimental analysis," *Mol. Syst. Biol.*, vol. 2, p. 41, 2006.

[8] D. Nevozhay, R. M. Adams, K. F. Murphy, K. Josic, and G. Balazsi, "Negative autoregulation linearizes the dose response and suppresses the heterogeneity of gene expression," *P. Natl. Acad. Sci. USA*, vol. 106, pp. 5123–5128, 2009.

[9] P. Bokes and A. Singh, "Gene expression noise is affected differentially by feedback in burst frequency and burst size," *J. Math. Biol.*, vol. 74, pp. 1483–1509, 2017.

[10] P. Bokes, Y. Lin, and A. Singh, "High cooperativity in negative feedback can amplify noisy gene expression," *B. Math. Biol.*, pp. doi: 10.1007/s11538–018–0438–y, 2018.

[11] N. Rosenfeld, M. B. Elowitz, and U. Alon, "Negative autoregulation speeds the response times of transcription networks," *J. Mol. Biol.*, vol. 323, pp. 785–793, 2002.

[12] M. L. Simpson, C. D. Cox, and G. S. Sayler, "Frequency domain analysis of noise in autoregulated gene circuits," *P. Natl. Acad. Sci. USA*, vol. 100, pp. 4551–4556, 2003.

[13] A. Becskei and L. Serrano, "Engineering stability in gene networks by autoregulation," *Nature*, vol. 405, pp. 590–593, 2000.

[14] P. S. Swain, "Efficient attenuation of stochasticity in gene expression through post-transcriptional control," *J. Mol. Biol.*, vol. 344, pp. 965–976, 2004.

[15] A. Singh, "Negative feedback through mRNA provides the best control of gene-expression noise," *IEEE T. NanoBiosci.*, vol. 10, pp. 194–200, 2011.

[16] M. Thattai and A. van Oudenaarden, "Intrinsic noise in gene regulatory networks," *P. Natl. Acad. Sci. USA*, vol. 98, p. 151588598, 2001.

[17] A. J. Stewart, R. M. Seymour, A. Pomiankowski, and M. Reuter, "Under-dominance constrains the evolution of negative autoregulation in diploids," *PLoS Comput. Biol.*, vol. 9, p. e1002992, 2013.

[18] L. Bleris, Z. Xie, D. Glass, A. Adadey, E. Sontag, and Y. Benenson, "Synthetic incoherent feedforward circuits show adaptation to the amount of their genetic template," *Mol. Syst. Biol.*, vol. 7, p. 519, 2011.

[19] M. Osella, C. Bosia, D. Corá, and M. Caselle, "The role of incoherent microRNA-mediated feedforward loops in noise buffering," *PLoS Comput. Biol.*, vol. 7, p. e1001101, 2011.

[20] J. Tsang, J. Zhu, and A. van Oudenaarden, "MicroRNA-mediated feedback and feedforward loops are recurrent network motifs in mammals," *Mol. Cell*, vol. 26, pp. 753–767, 2007.

[21] T. J. Strovas, A. B. Rosenberg, B. E. Kuypers, R. A. Muscat, and G. Seelig, "MicroRNA-based single-gene circuits buffer protein synthesis rates against perturbations," *ACS Synth. Biol.*, vol. 3, pp. 324–331, 2014.

[22] M. Soltani, T. Platini, and A. Singh, "Stochastic analysis of an incoherent feedforward genetic motif," in *American Control Conference (ACC)*, pp. 406–411, 2016.

[23] X. Li, J. J. Cassidy, C. A. Reinke, S. Fischboeck, and R. W. Carthew, "A microRNA imparts robustness against environmental fluctuation during development," *Cell*, vol. 137, pp. 273–282, 2009.

[24] C. Bosia, M. Osella, M. E. Baroudi, D. Cora, and M. Caselle, "Gene autoregulation via intronic microRNAs and its functions," *BMC Syst. Biol.*, vol. 6, p. 131, 2012.

[25] T. Platini, T. Jia, and R. V. Kulkarni, "Regulation by small RNAs via coupled degradation: Mean-field and variational approaches," *Phys. Rev. E*, vol. 84, p. 021928, 2011.

[26] N. Kumar, T. Jia, K. Zarringhalam, and R. V. Kulkarni, "Frequency modulation of stochastic gene expression bursts by strongly interacting small RNAs," *Phys. Rev. E*, vol. 94, p. 042419, 2016.

[27] J. M. Schmiedel, S. L. Klemm, Y. Zheng, A. Sahay, N. Blüthgen, D. S. Marks, and A. van Oudenaarden, "MicroRNA control of protein expression noise," *Science*, vol. 348, pp. 128–132, 2015.

[28] T. Jahnke and W. Huisinga, "Solving the chemical master equation for monomolecular reaction systems analytically," *J. Math. Biol.*, vol. 54, pp. 1–26, 2007.

[29] F. P. Kelly, *Reversibility and stochastic networks*. Cambridge University Press, 2011.

[30] D. F. Anderson, G. Craciun, and T. G. Kurtz, "Product-form stationary distributions for deficiency zero chemical reaction networks," *B. Math. Biol.*, vol. 72, pp. 1947–1970, 2010.

[31] D. F. Anderson and S. L. Cotter, "Product-form stationary distributions for deficiency zero networks with non-mass action kinetics," *B. Math. Biol.*, vol. 78, pp. 2390–2407, 2016.

[32] G. C. Innocentini, S. Guiziou, J. Bonnet, and O. Radulescu, "Analytic framework for a stochastic binary biological switch," *Phys. Rev. E*, vol. 94, p. 062413, 2016.

[33] G. C. Innocentini, M. Forger, O. Radulescu, and F. Antoneli, "Protein synthesis driven by dynamical stochastic transcription," *B. Math. Biol.*, vol. 78, pp. 110–131, 2016.

[34] T. Zhou and T. Liu, "Quantitative analysis of gene expression systems," *Quant. Biol.*, vol. 3, pp. 168–181, 2015.

[35] H. Pendar, T. Platini, and R. V. Kulkarni, "Exact protein distributions for stochastic models of gene expression using partitioning of Poisson processes," *Phys. Rev. E*, vol. 87, p. 042720, 2013.

[36] X. Yang, Y. Wu, and Z. Yuan, "Characteristics of mRNA dynamics in a multi-on model of stochastic transcription with regulation," *Chinese J. Phys.*, vol. 55, pp. 508–518, 2017.

[37] A. Singh, C. A. Vargas-Garcia, and R. Karmakar, "Stochastic analysis and inference of a two-state genetic promoter model," *P. Amer. Contr. Conf.*, pp. 4563–4568, 2013.

[38] L. Cardelli, M. Kwiatkowska, and L. Laurenti, "Stochastic analysis of chemical reaction networks using linear noise approximation," *Biosystems*, vol. 149, pp. 26–33, 2016.

[39] E. Cinquemani, "On observability and reconstruction of promoter activity statistics from reporter protein mean and variance profiles," in *International Workshop on Hybrid Systems Biology*, pp. 147–163, Springer, 2016.

[40] N. Herath and D. Del Vecchio, "Reduced linear noise approximation for biochemical reaction networks with time-scale separation: The stochastic tQSSA+," *J. Chem. Phys.*, vol. 148, p. 094108, 2018.

[41] L. Bronstein and H. Koeppl, "A variational approach to moment-closure approximations for the kinetics of biomolecular reaction networks," *J. Chem. Phys.*, vol. 148, p. 014105, 2018.

[42] A. Singh and R. Grima, "The linear-noise approximation and moment-closure approximations for stochastic chemical kinetics," *arXiv preprint arXiv:1711.07383*, 2017.

[43] K. R. Ghusinga, C. A. Vargas-Garcia, A. Lamperski, and A. Singh, "Exact lower and upper bounds on stationary moments in stochastic biochemical systems," *Phys. Biol.*, vol. 14, p. 04LT01, 2017.

[44] M. Soltani, C. A. Vargas-Garcia, and A. Singh, "Conditional moment closure schemes for studying stochastic dynamics of genetic circuits," *IEEE T. Biomed. Circ. S.*, vol. 9, pp. 518–526, 2015.

[45] X. Lai, O. Wolkenhauer, and J. Vera, "Understanding microrna-mediated gene regulatory networks through mathematical modelling," *Nucleic Acids Res.*, vol. 44, no. 13, pp. 6019–6035, 2016.

[46] S. Grigolon, F. Di Patti, A. De Martino, and E. Marinari, "Noise processing by microrna-mediated circuits: the incoherent feedforward loop, revisited," *Heliyon*, vol. 2, no. 4, p. e00095, 2016.

[47] A. Carignano, S. Mukherjee, A. Singh, and G. Seelig, "Extrinsic noise suppression in micro rna mediated incoherent feedforward loops," in *2018 IEEE Conference on Decision and Control (CDC)*, pp. 4353–4359, IEEE, 2018.

[48] L. Laurenti, A. Csikasz-Nagy, M. Kwiatkowska, and L. Cardelli, "Molecular filters for noise reduction," *Biophys. J.*, vol. 114, no. 12, pp. 3000–3011, 2018.

[49] T. G. Kurtz, "The relationship between stochastic and deterministic models for chemical reactions," *J. Chem. Phys.*, vol. 57, pp. 2976–2978, 1972.

[50] D. Kendall, "Stochastic processes and population growth," *J. Roy. Stat. Soc. B*, vol. 11, pp. 230–82, 1949.

[51] P. Bokes, J. R. King, A. T. Wood, and M. Loose, "Exact and approximate distributions of protein and mRNA levels in the low-copy regime of gene expression," *J. Math. Biol.*, vol. 64, pp. 829–854, 2012.

[52] X. Kan, C. H. Lee, and H. G. Othmer, "A multi-time-scale analysis of chemical reaction networks: II. stochastic systems," *J. Math. Biol.*, vol. 73, pp. 1081–1129, 2016.
[53] A. Singh and P. Bokes, "Consequences of mRNA transport on stochastic variability in protein levels," *Biophys. J.*, vol. 103, pp. 1087–1096, 2012.
[54] I. Lestas, J. Paulsson, N. Ross, and G. Vinnicombe, "Noise in gene regulatory networks," *IEEE T. Circuits-I*, vol. 53, pp. 189–200, 2008.
[55] M. Feinberg, "Lectures on chemical reaction networks. Notes of lectures given at the Mathematics Research Center of the University of Wisconsin," 1979.
[56] W. Abou-Jaoudé, D. Thieffry, and J. Feret, "Formal derivation of qualitative dynamical models from biochemical networks," *Biosystems*, vol. 149, pp. 70–112, 2016.
[57] J. Paulsson, "Models of stochastic gene expression," *Phys. Life Rev.*, vol. 2, pp. 157–175, 2005.
[58] N. van Kampen, *Stochastic Processes in Physics and Chemistry*. Elsevier, 2006.
[59] D. Gillespie, "A General method for numerically simulating stochastic time evolution of coupled chemical reactions," *J. Comput. Phys.*, vol. 22, pp. 403–34, 1976.
[60] T. R. Maarleveld, B. G. Olivier, and F. J. Bruggeman, "StochPy: A comprehensive, user-friendly tool for simulating stochastic biological processes," *PLoS ONE*, vol. 8, p. e79345, 2013.
[61] F. Zhang and D. Wang, "The pattern of microRNA binding site distribution," *Genes*, vol. 8, p. 296, 2017.

Pavol Bokes received his master's degree in mathematics from Comenius University in Bratislava, Slovakia, and his doctoral degree in mathematical biology from University of Nottingham in Nottingham, United Kingdom. Since 2010 we works at Comenius University: initially in the position of Assistant Professor; and, after his habilitation in 2015, as an Associate Professor in mathematics.

Michal Hojcka received his bachelor's and master's degrees in mathematical finance and a doctoral degree in applied mathematics from Comenius University in Bratislava, Slovakia. He works in the private sector.

Abhyduai Singh earned his bachelors degree in mechanical engineering from the Indian Institute of Technology in Kanpur, India. He received masters degrees in both mechanical and electrical & computer engineering from Michigan State University, and a masters degree in ecology, evolution and marine biology from University of California Santa Barbara (UCSB). After earning his doctoral degree in electrical & computer engineering in 2008, also from UCSB, he completed postdoctoral work in UC San Diegos Department of Chemistry and Biochemistry. Since 2017 he is an Associate Professor in Electrical & Computer Engineering, and Biomedical Engineering at the University of Delaware.